Bioconjugate Chemistry

Article

Cite This: Bioconjugate Chem. 2019, 30, 1371−1384

pubs.acs.org/bc

Penetration and Uptake of Nanoparticles in 3D Tumor Spheroids

Aleksandra Tchoryk,[†,‡] Vincenzo Taresco,[†] Richard H. Argent,[†] Marianne Ashford,[§] Paul R. Gellert,[∥] Snow Stolnik,[†] Anna Grabowska,[‡] and Martin C. Garnett*[,†]

[†]Division of Molecular Therapeutics and Formulation, School of Pharmacy, [‡]Cancer Biology Unit, Division of Cancer and Stem Cells, University of Nottingham, Nottingham NG7 2RD, United Kingdom

[§]Advanced Drug Delivery, Pharmaceutical Sciences, IMED Biotech Unit, AstraZeneca, Macclesfield SK10 2NA, United Kingdom

[∥]Innovation Strategies and External Liaison, Pharmaceutical Technology and Development, AstraZeneca, Macclesfield, SK10 2NA, United Kingdom

Supporting Information

ABSTRACT: Animal models are effective for assessing tumor localization of nanosystems but difficult to use for studying penetration beyond the vasculature. Here, we have used well-characterized HCT116 colorectal cancer spheroids to study the effect of nanoparticle (NP) physicochemical properties on penetration and uptake. Incubation of spheroids with Hoechst 33342 resulted in a dye gradient, which facilitated discrimination between the populations of cells in the core and at the periphery of spheroids by flow cytometry. This approach was used to compare doxorubicin and liposomal doxorubicin (Caelyx) and a range of model poly(styrene) nanoparticles of different sizes (30 nm, 50 nm, 100 nm) and with different surface chemistries (50 nm uniform plain, carboxylated, aminated and a range of NPs and polyethylene glycol modified NPs prepared from a promising new functionalized biodegradable polymer (poly(glycerol-adipate), PGA). Unmodified poly(styrene) nanoparticles (30 nm/50 nm) were able to penetrate to the core of HCT116 spheroids more efficiently than larger poly(styrene) nanoparticles (100 nm). Surprisingly, penetration of 30 and 50 nm particles was as good as clinically relevant doxorubicin concentrations. However, penetration was reduced with higher surface charge. PGA NPs of 100 nm showed similar penetration into spheroids as 50 nm poly(styrene) nanoparticles, which may be related to polymer flexibility. PEG surface modification of polymeric particles significantly improved penetration into the spheroid core. The new model combining the use of spheroids Hoechst staining and flow cytometry was a useful model for assessing NP penetration and gives useful insights into the effects of NPs' physical properties when designing nanomedicines.

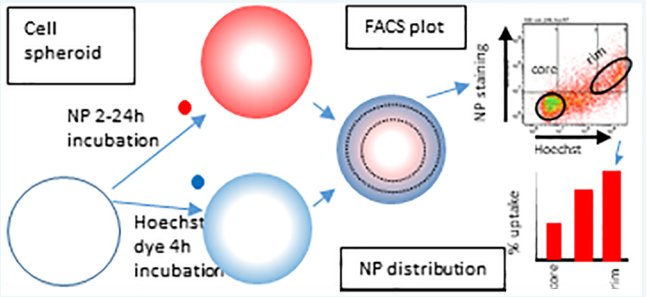

There has been great interest in using nanoparticle systems to deliver anticancer drugs into tumors as they offer advantages such as selective accumulation at the tumor site, with potential for enhanced efficacy and reduced toxicity compared to conventional drug treatment. Much of the justification for the use of nanoparticles is based on the enhanced permeability and retention effect, which proposes that macromolecules and nanoparticles accumulate in tumors due to a leaky vasculature and absence of a lymphatic system. Variation in vascular leakiness in different types and different areas of the same tumor can lead to limited accumulation in tumors and lowers the effectiveness of the treatments.[1] The heterogeneous distribution in tumors is thought to be a reason why Doxil and Abraxane, nanosystems which have been FDA-approved for cancer, demonstrate disappointing treatment benefits in poorly vascularized tumors.[2,3] However, this is just the first step of reaching the target cells, and penetration through the tumor extracellular matrix (ECM) and uptake into tumor cells is at least as important. There is a limited amount of data in the literature on how the ECM impacts various nanosystems, but there are several examples of poor penetration into tumors resulting in poor performance of these novel therapeutics.[4−7]

The ability of drug molecules and nanosystems to reach their target cells may be affected by the complex physiology of the tissue. Tumors consist of cancer cells and supportive stroma which includes an ECM bathed in an extra cellular fluid. The extracellular fluid can constitute in excess of 20% of the tumor volume.[8] The ECM is a meshwork made of collagen fibers, proteoglycans, or glycosamino glycans such as hyaluronic acid and heparan sulfate forming a highly viscous and negatively charged barrier.[9−11] These components are thought to largely prevent convective flow within the tumor matrix, meaning that molecules move through the matrix by diffusion, thus limiting the rate of movement of molecules and nanomaterials through the tumor tissue.[12−14] However, there

Received: February 18, 2019
Revised: April 3, 2019
Published: April 4, 2019

DOI: 10.1021/acs.bioconjchem.9b00136
Bioconjugate Chem. 2019, 30, 1371−1384

are lower levels of proteoglycans and hyaluronate present within tumors.[8] Additionally, steric factors and electrostatic interactions due to repulsion and binding to the ECM components will influence the rate of movement.[15,16] There is, however, a need to develop a better understanding of how these interactions affect the delivery of drugs and nanosystems into tumors and whether these delivery systems can be optimized to minimize these effects.

The current process for testing the effectiveness of nanosystems relies greatly on animal models. However, the animal models that are readily available such as the human tumor xenograft or genetically engineered mouse models are technically difficult, expensive, and time-consuming to use and poorly representative of the clinical disease. Additionally, it is more difficult to achieve the resolution needed to see penetration at the cellular and tissue level, and so these models will be less useful for understanding and inappropriate for mass screening of nanodelivery systems. If we are to develop a rational design of nanoparticles (NPs), there is a need for representative *in vitro* models and screening methods that will allow the testing of penetrability of nanomedicines in the early stages of the drug development process. While the *in vitro* model should mimic the *in vivo* tumor microenvironment as far as possible, it also should be simple and easy to reproduce and analyze.[17] We have chosen to work with 3D human tumor spheroids as a model for solid tumors as they are believed to more closely resemble the tumor microenvironment.[18−21] They have a 3D spatial arrangement with enhanced cell to cell contact and the ability to form proliferative gradients, hypoxia, and necrosis. Certain ECM components were found to be expressed at high levels in 3D spheroids, hence they have the potential to establish the penetration barriers seen *in vivo*, thereby allowing us to study the penetration, distribution, and uptake of nanoparticles within these models.[22−25] However, to date, there are limited numbers of studies that employ tumor spheroids for the evaluation of nanomedicines.

Although there is increasing evidence indicating that the physicochemical properties of NPs such as size, charge, and surface chemistry play a crucial role in their ability to penetrate through the ECM, the effect of these physicochemical properties on penetration and uptake in representative tumor models has not been examined systematically.[2,15,26]

In the present study, we have taken well characterized human tumor spheroids and developed a convenient methodology to assess the penetration of nanoparticles into these spheroids. We have examined the effects of the size, surface, and bulk characteristics of a range of NPs on the penetration and cellular uptake into tumors. We have compared a typical anticancer drug, doxorubicin (DOX), with a clinically available liposomal doxorubicin with a size of ∼87 nm, Caelyx (a poly(ethylene glycol)ated (PEGylated) liposomal formulation of DOX also marketed as Doxil). We have used well characterized poly(styrene) latices as model NPs to assess the effects of size and charge. Finally, we have employed a range of NPs prepared from some new experimental biodegradable polymers with different acyl and polyethylene glycol modifications to assess their transport properties in spheroids. From these various results, we aim to identify the features that facilitate penetration of the nanosystems into cancer tissue, thereby leading to development of drug delivery systems with improved therapeutic performance.

RESULTS

3D Spheroid Model. The HCT116 colorectal spheroids used in this study were based on the methodology described by Ivanov et al.[25] and, as in the previous work with brain tumor cells, formed tight spheroids at day 3 of the culture with a defined border. The spheroids had an average diameter of 430 μm (Figure 1 A) and were very reproducible with a coefficient

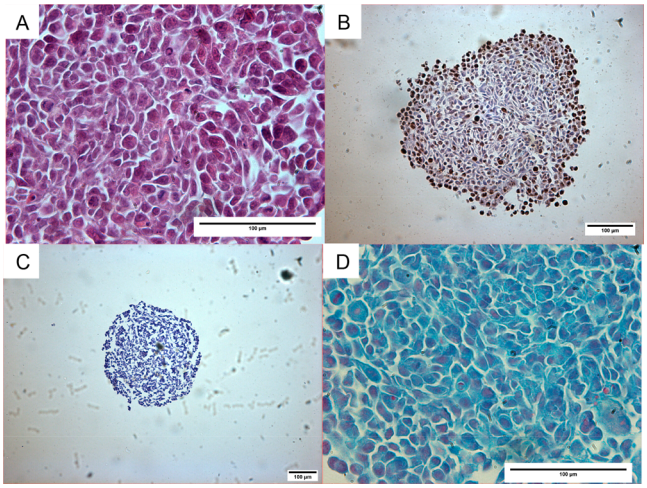

Figure 1. Immunohistological assessment of HCT116 spheroid microenvironment; 4 μm paraffin cross-section stained with (A) haematoxylin and eosin showing spheroid morphology and compaction; (B) proliferation marker K_i = 67, brown staining (peroxidase) showing proliferating cells; (C) pimonidazole, a lack of staining (brown) indicates absence of hypoxic regions; (D) Alcian Blue/fast red showing strongly acidic sulfated mucosubstances, blue; nuclei, pink to red; cytoplasm, pale pink. Scale bar 100 μm.

of variation in spheroid diameter ≤ 6% (n = 6) on day three after seeding. The variation in spheroids size between independent plates on day 3 was CV ≤ 5%.

Further, the immunohistochemical analysis revealed that spheroids consisted of layers of tightly packed, mainly viable proliferating cells with no necrotic core or hypoxia present (Figure 1A−C). Additionally, Alcian Blue staining showed the presence of sulfated and carboxylated acid glycosaminoglycans and sulfated and carboxylated sialomucins (Figure 1D). Having glycosaminoglycans present in HCT116 spheroids indicates the presence of an extracellular matrix and suggests that they should present a similar penetration barrier to that seen in vivo. While different tumors may be expected to have a range of different absolute penetration characteristics, a model containing the appropriate components should allow a realistic comparison between the penetration characteristics of different types of particles.

Optimization of Flow Cytometry/Hoechst Method. A qualitative picture of NP penetration can be obtained using confocal microscopy imaging of spheroids. However, this suffers from an increasing quenching of fluorescence with increasing depth from the spheroid surface, and it is tedious to cut histological sections to derive data from the whole spheroid routinely. In order to quantify the penetration and uptake of NPs in a convenient and robust manner, we have adopted a flow cytometry analysis method using Hoechst 33342 dye. The Hoechst dye is a nuclear stain which forms a noticeable diffusion/consumption gradient as it diffuses through spheroids. Therefore, at an appropriate concentration, the dye

DOI: 10.1021/acs.bioconjchem.9b00136
Bioconjugate Chem. 2019, 30, 1371−1384

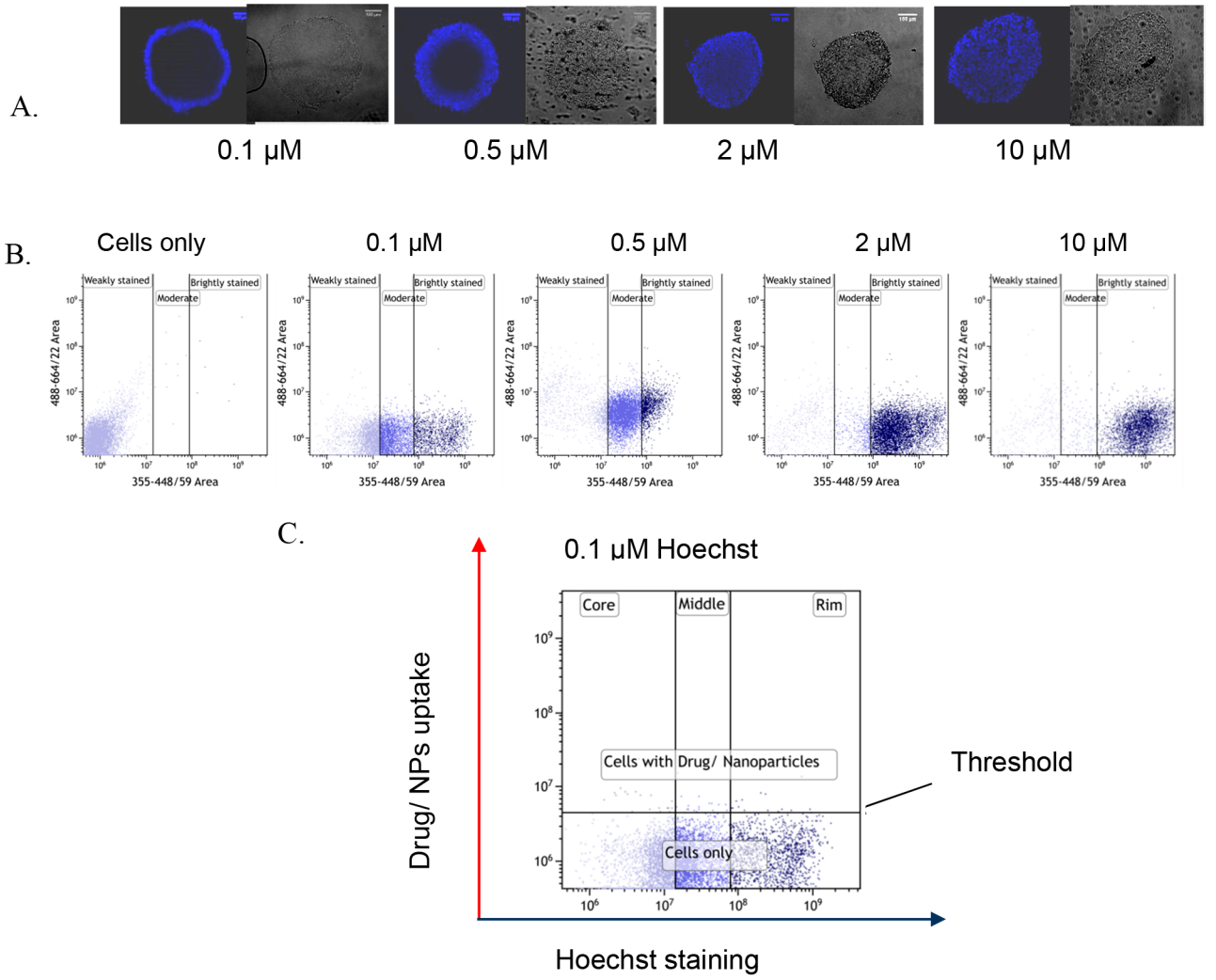

Figure 2. Concentration-dependent penetration of Hoechst in HCT116 spheroids incubated with 0.1 μM, 0.5 μM, 2 μM, and 10 μM of Hoechst for 4 h (blue, nuclei stained with Hoechst). (A) Confocal images representing the degree of staining of spheroids at different concentrations of Hoechst in comparison with Bright field views showing the extent of the spheroid. (B). FACS plots showing the distribution of HCT116 cells using varying concentrations of Hoechst and representing the distribution of cells based on the degree of staining at each concentration. (C) FACS dot plot of HCT116 spheroids stained with 0.1 μM Hoechst. The dye forms a diffusion gradient in spheroids that can be divided into three segments: 40% (±1%) unstained cell population representing the core, 20% (± 1%) brightest cells representing periphery, and 40% (±1%) weakly stained, representing cells between the rim and core of spheroids.

stains cells at the periphery of the spheroid to a greater extent than the cells within the core of the spheroid. The technique was previously used by Durand et al. for the selection of populations of cells with different proliferative statuses in spheroids after drug treatment and was found to be highly sensitive and reproducible. The dye has also been employed *in vivo* for localization of tissue near blood vessels.[27]

In the present work, we optimized Hoechst staining for gradient formation by incubating HCT116 spheroids with different concentrations of the dye (Figure 2 A, B). Concentration-dependent penetration was observed, with 0.1 μM dye concentration forming a fluorescent gradient that, following cell disaggregation and fluorescence activated cell sorter (FACS) analysis, could be divided into three concentric segments based on the fluorescence intensity of the cells. Unstained cells (40% (±1%) of total cell population) representing cells within the center of the spheroid; the brightest 20% (±1%) of the total cell population representing cells at the rim of spheroids and weakly stained cells located in a middle segment between the center and the rim (40% (±1%) of cell population; Figure 2C,D). (From calculations of volumes of a sphere, the unstained core corresponds to an inner radius of approximately 160 μm, the middle weakly stained segment a ring of a further 40 μm depth, and the brightly stained rim the outside 15 μm thickness of an average spheroid.) Once the Hoechst concentration was selected, the spheroids were incubated with fluorescently labeled nanoparticles (2, 4, 6 and 24 h) and with the dye (4 h) to determine time-dependent penetration and uptake of these nanoparticles in HCT116 spheroids. The spheroids were dissociated into individual cells, fixed, and assayed by flow cytometry. It should be noted that as the cells are dissociated for the FACS quantitation, we will detect only the particles which both penetrate the spheroid and are taken up into cells.

Penetration and Uptake of Doxorubicin in HCT116 Spheroids. To compare the relative penetration of nanoparticles with a drug, DOX was chosen as a relevant marker. DOX would be expected to behave similarly to Hoechst dye,

DOI: 10.1021/acs.bioconjchem.9b00136
Bioconjugate Chem. 2019, 30, 1371−1384

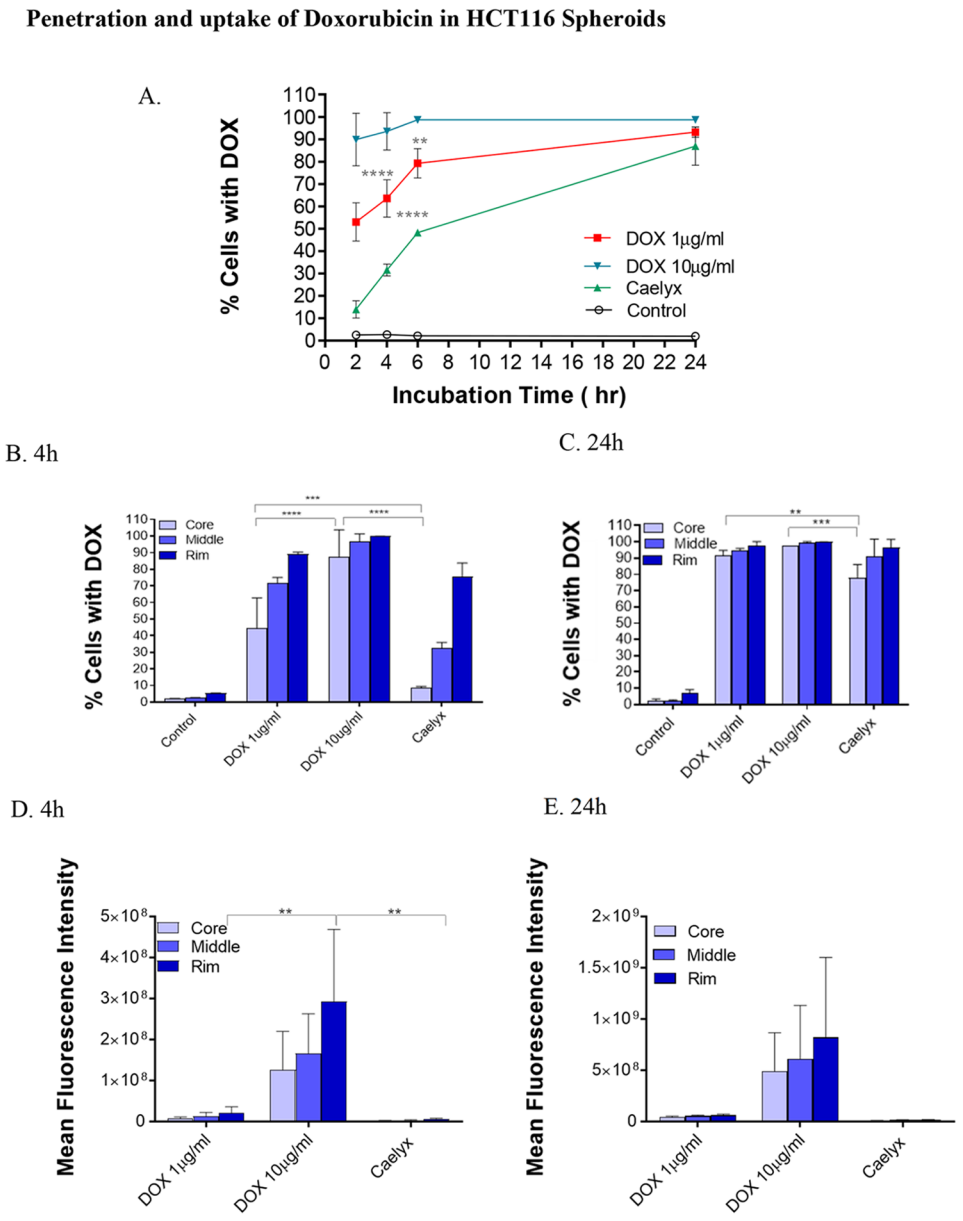

Figure 3. Penetration and uptake of doxorubicin and Caelyx in HCT116 spheroids. (A) Time-dependent penetration of DOX (1 μg/mL and 10 μg/mL) and Caelyx (providing 75 μg/mL of free DOX) in HCT116 spheroids by FACS. (B, C) Percentage of cells reached by the free DOX and Caelyx to different regions in spheroids after 4 and 24 h incubation time. (D, E) MFI plots showing accumulation of amounts of DOX and Caelyx per cell across the core, middle, and rim in HCT116 spheroids after 4 and 24 h incubation (****, ***, **, and * indicate $p < 0.0001$, $p < 0.001$, $p < 0.01$, and $p < 0.05$, respectively). Control values are background fluorescence of untreated cells.

being a DNA-binding lipophilic molecule of similar molecular weight. This makes it a particularly good example for determining the penetration of a potent anticancer drug in our model. Additionally, DOX is the drug component of the nanoscale liposomal formulation Caelyx, so we can determine the penetration of a clinically approved nanoparticulate formulation of the same drug with well-described *in vivo* properties in our model. Further, free DOX is fluorescent, which allows for easy detection via confocal microscopy and FACS.

The penetration and distribution of free DOX were evaluated in HCT116 spheroids after exposing the cells to different concentrations of the drug at 1 μg/mL and 10 μg/mL for different incubation periods, 4 and 24 h. These concentrations were chosen to be relevant to the clinical context, as the plasma mean concentration of free DOX in patients receiving a single intravenous dose of DOX solution is 0.2 μg/mL after 1 h and 0.1 μg/mL after 4 h, after which it reaches a plateau and remains at this level for 24 h.[28,29] Thus, in our study, the lower concentration of the free DOX (1 μg/mL) is closer to the drug concentration achieved clinically than the higher concentration of 10 μg/mL. The results were quantified by the FACS/Hoechst method in Figure 3A–E. Two different measures have been used to assess penetration into spheroids: first, the percentage of cells with a label, which counts any cell with a level of dye/drug above the background showing the extent of penetration, and second, the mean

DOI: 10.1021/acs.bioconjchem.9b00136
Bioconjugate Chem. 2019, 30, 1371–1384

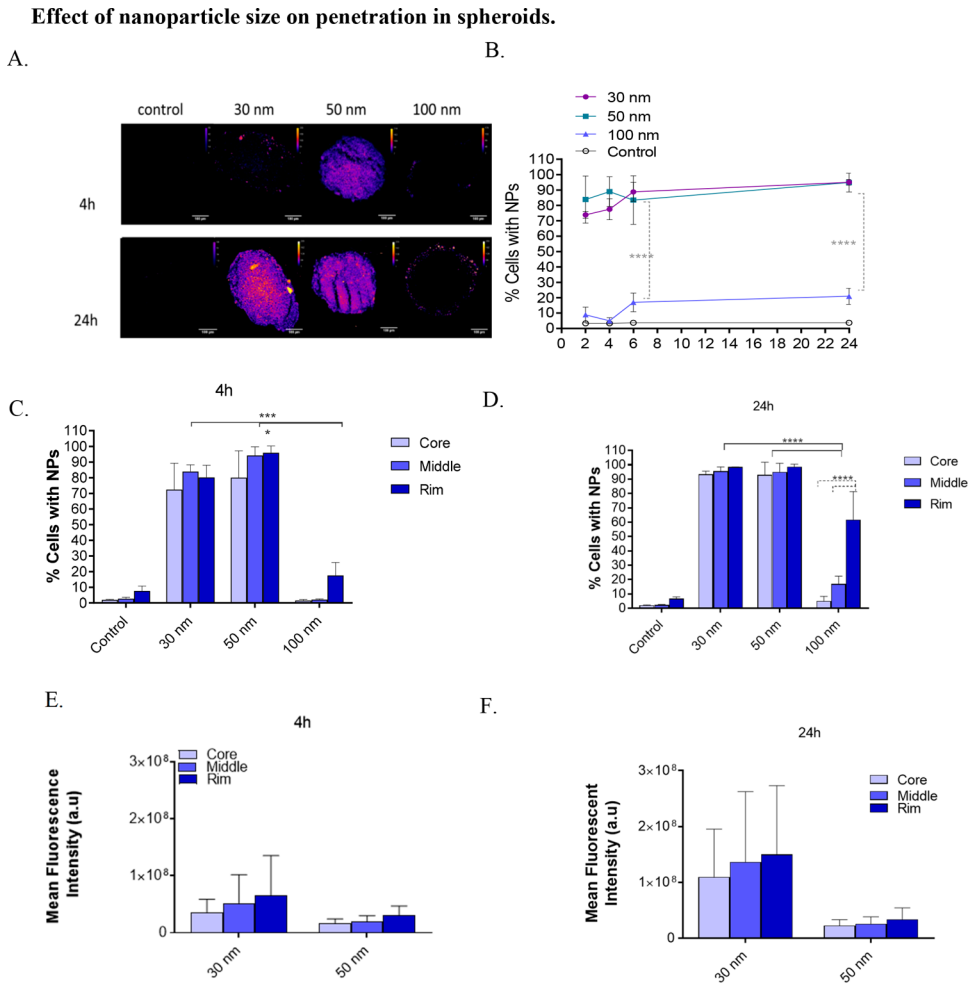

Figure 4. Size-dependent penetration of NPs into spheroids. (A) Confocal images of frozen sections (sections = 20 μm thickness) of HCT116 spheroids incubated with 30, 50, and 100 nm unmodified poly(styrene) nanoparticles (75 μg/mL). Scale bar 100 μm. Images processed to normalize fluorescence intensity by applying LUT fire in ImageJ software. (B) Time-dependent penetration of NPs in spheroids by FACS/Hoechst method. (C) Distribution of NPs in spheroids 4 h. (D) Distribution of NPs in spheroids 24 h. (E) Accumulation of nanoparticles in HCT116 spheroids measured by the MFI of nanoparticles after 4 h and (F) 24 h incubation. Control values are background fluorescence of untreated cells. (****, ***, **, and * indicate $p < 0.0001$, $p < 0.001$, $p < 0.01$, and $p < 0.05$, respectively).

fluorescence intensity (MFI) of cells, which is related to the average uptake of dye/drug in a particular population of cells.

Penetration of free DOX into HCT116 spheroids was time-dependent as well as concentration-dependent. At the lower dose of 1 μg/mL, the free DOX was detectable in around 50% of cells within the first 2 h, steadily increasing up to 80% of cells after 6 h incubation time and then increasing more gradually to reach 90% of cells in the spheroid by 24 h.

At the earlier time point (4 h), many more cells in the outer parts of the spheroid had taken up the drug than in the core of the spheroid (Figure 3B and C). A much higher number of cells taking up the drug toward the center of the spheroid was observed after 24 h of incubation. On the basis of the MFI, it is clear that the uptake of DOX across spheroids at 1 μg/mL is low and decreases toward the core (Figures 3D and E).

Penetration and Uptake of Doxorubicin in HCT116 Spheroids. By increasing concentration of the free DOX to 10 μg/mL, significantly faster delivery into the core of spheroid was achieved, with over 80% cells reached after only 2 h of incubation. The drug was associated with more than 90% of cells after 6 h of incubation. The uptake of free DOX at 10 μg/mL in the cells across the spheroid was still observed to be lower in the core at the early time point, 4 h, with a similar percentage of cells in each region having taken up DOX after 24 h. The higher concentration of DOX resulted in much higher accumulation of the drug in cells than the lower dose as quantified in Figure 3A–E. Additional original data of the FACS dot plots are given in Supporting Information Figure S1.

As a comparison, penetration and uptake of a liposomal formulation of DOX has been evaluated for the ability to deliver DOX to the colorectal spheroids. The formulation was tested at a concentration providing 75 μg/mL with respect to DOX, which is higher than the mean concentration of ~25 μg/mL achieved in plasma in patients receiving a single dose of Caelyx. The higher concentration was necessary in the study due to the technical inability to detect fluorescence in cells at a lower concentration. As seen in Figure 3A, the penetration profile of DOX via this nanoformulation was also found to be time-dependent. The diffusion of DOX as Caelyx in the HCT116 spheroid was very slow with less than 10% of cells containing DOX after 2 h incubation and 85% after 24 h incubation. As in the case of the free DOX, there was a large difference in the percentage of cells taking up Caelyx as measured by DOX fluorescence within the different spheroid

DOI: 10.1021/acs.bioconjchem.9b00136
Bioconjugate Chem. 2019, 30, 1371–1384

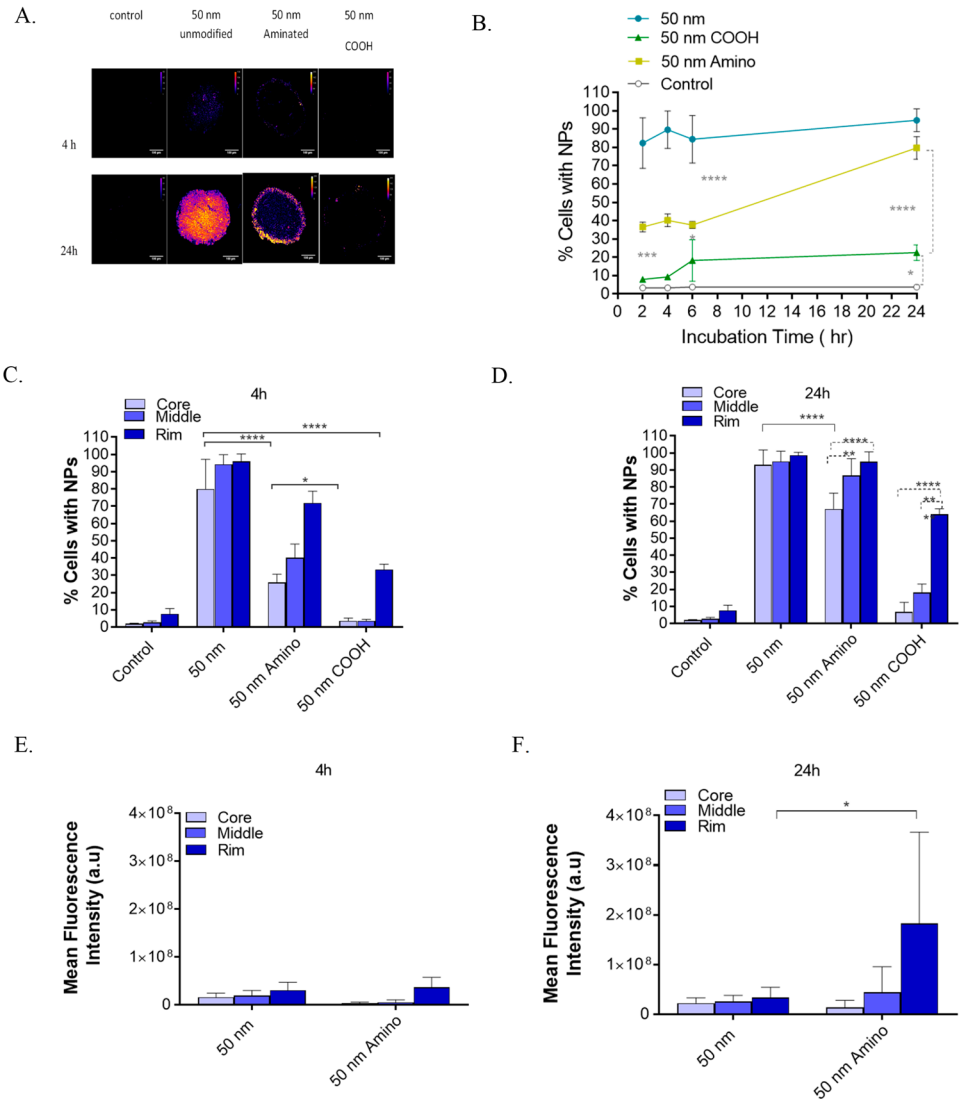

Figure 5. (A) Influence of NP surface charge on penetration of NPs into spheroids. Confocal images of frozen sections (sections = 20 μm) of HCT116 spheroids incubated with 50 nm of unmodified, aminated, and carboxylated poly(styrene) nanoparticles. Images processed to normalize fluorescence intensity by applying LUT fire based on the fluorescent intensity in ImageJ software. (B) Time-dependent penetration of NPs in spheroids. (C) Distribution of NPs in spheroids. (D) Distribution of NPs in spheroids after 24 h. (E) Accumulation of nanoparticles in HCT116 spheroids measured by the MFI of nanoparticles after 4 h and (F) 24 h incubation. Control values are background fluorescence of untreated cells (****, ***, **, and * indicates $p < 0.0001$, $p < 0.001$, $p < 0.01$, and $p < 0.05$, respectively).

regions at the 4 h time points, whereas a more similar uptake of Caelyx was seen across all regions of spheroid after 24 h (Figure 3B,C). The results also demonstrated that penetration of Caelyx and uptake into the cells of the spheroid was significantly slower and with much lower accumulation of the drug than that of the free DOX, even without accounting for the much higher dose of DOX in Caelyx used in this experiment (Figure 3D,E). The high level of Dox in Caelyx used may raise concerns about the potential toxicity of this higher concentration of drug in the formulation and its effects on the model. However, we saw no evidence for this effect, either in terms of the cell numbers from the spheroid available for analysis or the quality of cells seen by FACS parameters, and the size of the spheroids did not noticeably decrease over the longer time period (a key measure of toxicity).[25] The lack of toxicity probably relates to the slower penetration and uptake of Caelyx as described above.

Effect of Nanoparticle Size on Penetration in Spheroids. To examine the effect of size and surface chemistry of NPs on trafficking into spheroids, poly(styrene) NPs were employed as model particles as they are available in a range of different sizes and with versatile surfaces, thus allowing for comparative study. The effect of the size of NPs on the penetration into HCT116 spheroids was evaluated by using 30, 50, and 100 nm uniform plain poly(styrene) latices [see Supporting Information Tables S1 and S2 for a summary of NP characteristics]. The size-dependent penetration and localization of NPs are qualitatively displayed by confocal images of 20 μm thick spheroid sections in Figure 4A and quantified by the FACS/Hoechst method in Figure 4B. In both the confocal microscopy images and in the FACS data, the

DOI: 10.1021/acs.bioconjchem.9b00136
Bioconjugate Chem. 2019, 30, 1371−1384

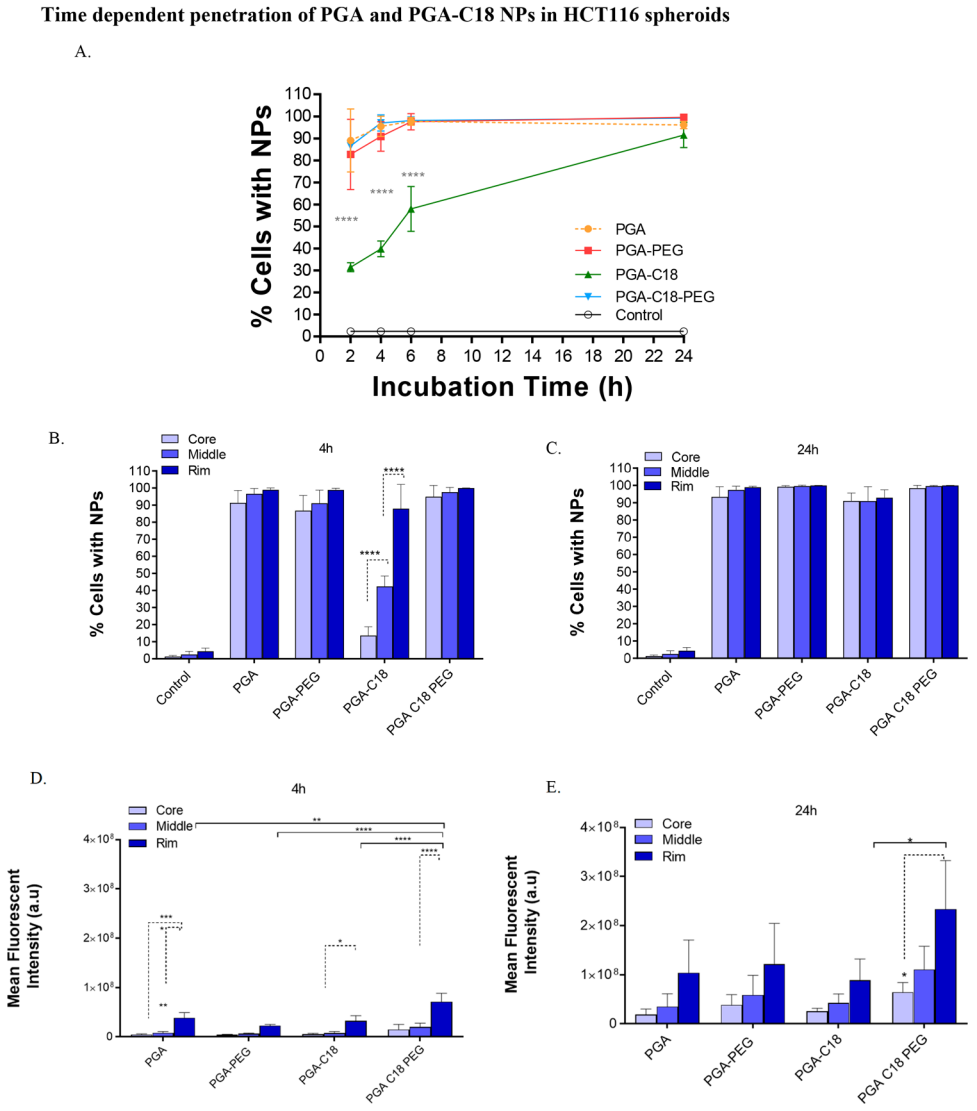

Figure 6. (A) Time-dependent penetration of PGA NPs in spheroids by FACS/Hoechst method. (B) Distribution of PGA NPs in spheroids after 4 h. (C) Distribution of PGA NPs in spheroids after 24 h. (D) Accumulation of PGA nanoparticles in HCT116 spheroids measured by the MFI of nanoparticles after 4 h of incubation and (E) after 24 h. The difference in MFI between the data was normalized by designating the PGA C18 NPs sample as equal to 1 and applying that adjustment factor to the remaining NPs by use of ratiometric results. Concentration of NPs = 75 μg/mL. Control values are background fluorescence of untreated cells (****, ***, **, and * indicate $p < 0.0001$, $p < 0.001$, $p < 0.01$, and $p < 0.05$, respectively).

fluorescence has been normalized between different systems (Supporting Information Figure S2 shows raw FACS data obtained in the dot plot format).

Small 30 nm NPs and 50 nm NPs were taken up in over 70% and 80% of cells, respectively, within the first 2 h of incubation, increasing to >90% of cells in the spheroid after a 6 h incubation. However, in the case of larger 100 nm nanoparticles, a different penetration profile was observed. Less than 10% of cells contained 100 nm NPs after 2 h of incubation, which further increased to a total of just 22% of cells after a 24 h incubation (Figure 4B).

Further, 30 and 50 nm nanoparticles were distributed evenly between the different concentric cell population segments based on Hoechst staining with ~80% of cells in the core segment of the spheroids taking up dye (Figure 4C,D). However, the 100 nm NPs were strongly associated with the periphery of spheroids with no significant penetration achieved in the core of spheroids even after the 24 h incubation period.

The results obtained by FACS correlate well with the results obtained by confocal imaging. The level of nanoparticle accumulation in the spheroids was investigated using the MFI normalized between the different NPs by designating a 50 nm NP sample as equal to 1 and applying an adjustment factor to the remaining NPs by use of ratiometric results. Figure 4E shows the uptake of 30 and 50 nm NPs in spheroids after 4 h incubation times. The plot shows a similar accumulation profile of the 30 and 50 nm particles, with slightly higher cell uptake achieved by 30 nm NPs. No significant difference in the amount of NPs uptake between the core, middle, and periphery of the spheroid was observed.

In Figure 4F, the accumulation profile for these NPs is presented after 24 h of incubation. It can be seen that while the MFI levels of 50 nm NPs remain similar to the ones observed after 4 h of incubation, the MFI of 30 nm increased considerably. This suggests that 50 nm NPs reached maximum accumulation in cells across the spheroid after 4 h of

DOI: 10.1021/acs.bioconjchem.9b00136
Bioconjugate Chem. 2019, 30, 1371−1384

incubation while 30 nm NPs continued to accumulate over a 24 h period. The MFI levels of 100 nm NPs were not investigated since these NPs do not penetrate far enough to accumulate in cells located deeper in the spheroid. Uniform uptake was observed for 30 and 50 nm NPs across the core, middle, and periphery of the spheroid after 24 h.

Effect of the Surface Charge of NPs on Penetration and Distribution in Spheroids. Next, we investigated the effect of nanoparticles with the same size of 50 nm but different surface charges: positively charged aminated and negatively charged carboxylated poly(styrene) nanoparticles in comparison to the unmodified plain poly(styrene) NPs on their ability to penetrate through spheroids. These more hydrophilic NPs were used as purchased and characterized by us before use (see Supporting Information Table S2).

When comparing these NPs, marked effects of the surface charge on penetration were observed. In the results by confocal microscopy, only 50 nm unmodified NPs were detectable within the core after 4 h of incubation while aminated 50 nm NPs showed preferential association with the periphery of spheroids. The 50 nm carboxylated nanoparticles were not taken up at a detectable level at this time. FACS confirmed that the penetration of the 50 nm unmodified nanoparticles into HCT116 spheroids was significantly faster and higher than that achieved by 50 nm aminated NPs (2×) or 50 nm carboxylated NPs (8×) after 4 h of incubation (Figure 5A,B; Supporting Information Figure S3 shows raw FACS data in dot plot format).

Effect of the Surface Charge of NPs on Penetration and Distribution in Spheroids. The penetration and uptake of 50 nm aminated NPs was found to be much slower and more time dependent than 50 nm unmodified NPs. The percent of cell uptake remained at <40% until 6 h of incubation. The percentage cells with detectable levels of NPs continued to increase, reaching ∼80% of cells after 24 h. Despite the overall high percentage of cell association of 50 nm aminated nanoparticles after 24 h, the distribution profile reveals significantly lower penetration and uptake in the core of spheroids compared to the outer layers after 24 h (Figure 5C,D).

The amount of cell uptake after 4 h of incubation as determined by MFI revealed a high uptake of 50 nm amine NPs in the rim of spheroids compared to the middle and core and also compared to plain NPs. At 24 h, these differences became more pronounced (Figure 5E and F).

Time Dependent Penetration of PGA and PGA-C18 NPs in HCT116 Spheroids. NPs were prepared using a solvent displacement method and were characterized for size and charge by DLS and zeta potential. The results showed that all formulations had a comparable mean diameter in the range of 109−117 nm when measured in deionized water and displayed a zeta potential around −30 in 10 mM HEPES similar to that of the plain poly(styrene) latices (for further details of PGA NP properties, see Supporting Information Tables S3 and S4).

Fast penetration of PGA NPs was observed with 80% cell association achieved after 2 h of incubation (Figure 6A−C). Significantly slower penetration for PGA-C18 NPs was observed than for PGA NPs with 30% cell association achieved after 2 h. The addition of a PEG group to PGA-C18 NPs significantly improved their penetration to a level similar to that of PGA alone or PGA−PEG (Supporting Information Figure S4 shows raw FACS data obtained in the dot plot format).

PGA NPs in HCT116 spheroids showed a greater preferential accumulation of NPs at the periphery than the middle or core (Figure 6D). NPs continued to accumulate with time in all parts of the spheroid. PEGylated PGA-C18 NPs showed significantly higher cell uptake in the cells at the rim of spheroids than other PGA NPs after both 4 h and 24 h incubation times (Figure 6E).

DISCUSSION

In the present study, a flow cytometry method utilizing a gradient of Hoechst staining as marker of cell position was optimized and successfully employed for quantitative analysis of penetration and distribution of different drugs and nanosystems in HCT116 spheroids. Only nanoparticles taken up into cells are detected, as nanoparticles still outside the cells will be lost on disaggregation. Previous work by us suggests that the great majority of NPs penetrating into spheroids are taken up by the cells;[30] however, there may be a small number of therapeutics which function at or bind to a non-endocytosable cell surface receptor which could not be tested in this model.

When considering the penetration of drug delivery systems into tumors, there are a number of different ways in which drugs and nanoparticles may penetrate into tumors. Drugs can usually diffuse and partition, so it is possible for drugs to easily enter cells as well as pass through the extracellular matrix by processes of diffusion and convection. NPs are not expected to pass across membranes but to be taken up into cells by endocytic processes and to be more restricted in passage through the ECM because of their size, the expected effects of size on diffusion, and a more restricted passage due to ECM porosity. Binding to charged ECM constituents and cell surfaces may also affect rates of transport and endocytosis. This study aimed to investigate some of these parameters using our new method.

It would be expected that the penetration of larger nanoparticles into tumor tissue may be less good than that of low molecular weight drugs, so the clinically relevant drug DOX and its clinically available liposomal counterpart Caelyx were investigated first to give some baselines for further comparisons. The results indicate that penetration of these systems was time and concentration dependent in HCT116 spheroids. A direct comparison with the Caelyx liposomal drug delivery system showed that penetration and uptake of Caelyx was considerably less effective than free DOX even after 24 h. This was not a surprising result considering that diffusion is inversely related to molecular weight. *In vivo* studies have also indicated that penetration of Caelyx into tumors is restricted.[31] This suggests that the model we have developed mirrors at least some characteristics of *in vivo* studies.

This account of liposome penetration is also similar to that of another HCT116 3D cell model where cells were seeded into hydrogel nested artificial cancer masses and left to mature for 7 days. In this latter model, both liposomes and micelles of <100 nm diameter also penetrated less well than free Dox.[32]

Next, we examined a number of other nanoparticle based systems to develop a better mechanistic understanding of the factors influencing nanoparticle penetration and uptake. First, we investigated the effects of both size and surface characteristics of model poly(styrene) nanoparticles on the penetration in spheroids. Our results showed that smaller nanoparticles (30

DOI: 10.1021/acs.bioconjchem.9b00136
Bioconjugate Chem. 2019, 30, 1371−1384

and 50 nm) showed greater penetration and accumulation in the core of HCT116 spheroids when compared to the larger (100 nm) nanoparticles. These results support our observations with the liposomal DOX (Caelyx) which appear to show a penetration somewhere between that of 50 and 100 nm poly(styrene) NPs and thus consistent with their size (~87 nm)

Our results are also consistent with the outcomes of previous *in vivo* and *in vitro* studies. Tang et al. compared the penetration abilities of 50 and 200 nm camptothecin-silica nanoparticle conjugates in the EL4 mouse T-lymphocyte tumor models *in vivo* and *ex vivo* and found higher penetration, accumulation, and internalization of the 50 nm nanoparticles in comparison to 200 nm particles that localized at the surface of tumors only.[2] These results suggest that the extracellular space together with the ECM matrix has a finite size restriction on nanoparticle penetration. It has been suggested that smaller nanoparticles are capable of diffusing through pores between the collagen fibrils, which have been measured to reach 20−40 nm in compact tumors and up to 75−130 nm in poorly organized tumors.[1433] This theory has been supported by previous studies which found that improved penetration of several therapeutic systems in solid tumors was achieved after the disruption of the ECM by the use of protease enzymes, collagenase, hyaluronidase, or drugs such as losartan.[5,13] However, it is still not clear how nanoparticle size relates to tumor penetration and cellular uptake. For instance, a study by Huang et al. found that for gold particles with a size below approximately 15 nm, there was better penetration than for larger particles.[34] Others also reported a difference in penetration capabilities between dendrimers with diameters of 2 and 4 nm/7 nm with the smallest showing better penetration than the 7 nm particle.[35] On the other hand, our results have demonstrated that in the present model particles up to 50 nm can successfully penetrate the tumor spheroids, and there is little difference in penetration characteristics compared to 30 nm NPs. These differences in penetration related to size reported in the literature may depend on the particular tumor model used for the study and differences in penetration mechanisms and factors affecting them.

The penetration of the 30 and 50 nm NPs were superior to that of DOX 1 μg/mL and similar to that of DOX 10 μg/mL. This is somewhat surprising as diffusion is inversely proportional to molecular weight, which suggests that larger nanoparticles would diffuse much more slowly than low molecular weight drugs.

Studies on the polysaccharide components of ECM suggest that at the concentrations present in ECM, they have an exclusion effect producing a colloid rich−water poor phase and a water rich−colloid poor phase, so that in terms of transport, larger molecules equilibrate faster than smaller molecules. ECM thus acts like a gel filtration chromatography column.[9] Our results showing longer times for accumulation of smaller drug molecules at the center of the spheroid in comparison to larger NPs which penetrated and accumulated in cells across the spheroid much faster fit well with these theories. In more recent work by Bao et al., it was proposed that liposomes of larger size and near neutral surface chemistry have decreased interactions with surrounding cells and ECM, and their movement is mediated by convection.[36] Jain et al. have also suggested that small molecules travel by diffusion, which is very restricted through the interstitial space; however, larger molecules (up to ECM pore size) can take advantage of movement by convection.[8] This implies that nanosystems with a small enough diameter and appropriate surface charge could penetrate into a tumor easily and be retained there over time.[37]

Although penetration of drugs through tissue is believed to be largely through the ECM, it will also be dependent on other factors such as binding to cells and tissue components, uptake into cells, and metabolism of the drugs.[5,38] In fact, the amount of both drug and NPs which are taken up and retained in cells strongly indicates that the process of cellular uptake would compete with penetration through the spheroid. The uptake of drugs and that of nanoparticles into cells are very different processes. For a drug like DOX, which readily diffuses across membranes and binds to DNA, there would be a strong equilibrium in favor of uptake and binding to DNA, whereas for NPs, which are taken up by the slower process of endocytosis, the balance is more likely to be in favor of further penetration into the spheroid, further advantaging the NPs in addition to any size exclusion effects. In considering whether DOX penetration may be limited by the amount of DOX bound to DNA in cells, some simple calculations have been carried out (see Supporting Information: Calculations on DOX Penetration into Spheroids). On the basis of the amount of DOX bound to cells at IC_{50}, if all the cells in the spheroid bound the expected amount of DNA, it would only account for about 1% of the DOX present in the well. However, the volume of the spheroid is only about 0.02% of the volume of the well, so the rate of diffusion of DOX to the cell may be a rate limiting step in comparison to the rate of uptake of DOX into the outer cells of the spheroid, thus reducing the rate of penetration. This explanation would be supported by our data showing that a 10× higher concentration of DOX readily penetrated the spheroid.

We also observed that penetration of the 50 nm poly(styrene) nanoparticles was strongly influenced by their surface characteristics. This suggests that other mechanisms in addition to size play a crucial role in the penetration and uptake process of nanoparticles. Indeed, it was proposed that charged components of ECM restrict the diffusion of positively and negatively charged particles due to electrostatic attraction and binding.[16] We have thus investigated the influence of the surface charge of the nanoparticles using NPs with the same 50 nm size but different surface charges: positively charged aminated NPs and negatively charged carboxylated NPs. These charged NPs are also more hydrophilic than the unmodified NPs. Our results show that penetration of these particles was strongly dependent on surface characteristics: whereas unmodified 50 nm nanoparticles were capable of penetration into the center of the spheroid (>200 μm depth), the negatively charged carboxylated NPs were incapable of penetrating further than one cell diameter from the rim. At a simple level, it could be argued that this exclusion from entering the spheroids is probably due to negative electrostatic repulsion from the negatively charged components of the ECM toward the negatively charged surface of both the spheroid and the cell surfaces. In our study, both plain and carboxylated nanoparticles had the same zeta potential in the HEPES buffer (−32 mV), and both became slightly negative −6 ± 0.7 and −9 ± 0.8, respectively, in RPMI-1640 medium supplemented with fetal bovine serum (FBS), conditions which were used for the studies. Despite similar characteristics shown by the zeta potential, the nanoparticles behaved very differently in the biological environment, thus affecting their ability to penetrate and accumulate in the spheroids. This is likely due to the

DOI: 10.1021/acs.bioconjchem.9b00136
Bioconjugate Chem. 2019, 30, 1371−1384

adsorption of a protein corona on the nanoparticle surface, which is shown by the increased size of the NPs by DLS when incubated in a medium plus FBS (See Supporting Information Table S2). Different surfaces can result in adsorption of different serum components, which may have different effects on NPs penetration and uptake but which are not defined at present in the context of spheroid models.[39]

The aminated NPs achieved a higher uptake into cells than carboxylated NPs, presumably due to interactions with negatively charged plasma membrane proteins on the cell surface.[8,16] However, their penetration through the spheroid was slow and limited to the outer cell layers of the spheroid, ~30−50 μm depth from the surface. This may be partly due to a "binding site effect" with the negatively charged ECM components, which hindered further diffusion. However, because of the increased cellular uptake of these positively charged NPs both in 2D and in 3D culture, it may be that the uptake of NPs into cells provides a larger barrier to penetration of these particles further into the spheroid similar to the binding site effect seen for penetration of tumor associated antibodies,[26,40,41] but in this case due to a less specific interaction. These results suggest that *in vivo*, these particles could deliver a high therapeutic dose to the most accessible cells but that cells deeper within the tumor may receive subtherapeutic drug concentrations, especially if the NPs are only present in the leaky vasculature for shorter periods. The penetration of smaller, slightly negative unmodified NPs was shown to penetrate easily into the core of spheroids, thus systems with this characteristic should be a better choice for cancer treatment.

To investigate a wider range of different nanoparticle properties, a series of novel biodegradable poly(glycerol adipate) (PGA) polymers which offer promising, new materials for NP fabrication were also tested for their penetration ability in 3D spheroids.[42−46] PGA has on average one terminal carboxyl group per chain, so it is expected to have some surface hydrophilic character, and this is reflected in the negative zeta potential of these nanoparticles (see Supporting Information Table S4).

The results showed that unmodified PGA NPs of approximately 100 nm diameter were able to penetrate to the core of the spheroids after only 2 h of incubation, reaching 90% of the cells. However, when the PGA polymer was modified with oleate (C18) moieties, the resulting NPs showed significantly slower penetration into spheroids and restricted distribution across all regions of the spheroids. The size and charge of those two types of NPs were comparable, which indicates that other physicochemical features influenced the behavior of these NPs. By modifying the PGA via partial esterification of the pendant hydroxyl group with the acid chloride of fatty acids, a material with very different characteristics and composition is produced. It was shown through measurement of the contact angle that the hydrophobicity of PGA increased with increased substitution and length of acyl chains. Further, PGA substituted with C18 groups resulted in a semi crystalline character.[47,30] Mackenzie et al. found in computational studies that when this polymer is used for NP formulation, the C18 groups arrange themselves toward the inside of the nanoparticle.[48] This indicates that the hydrophobicity on the surface of the nanoparticle should not be affected significantly. We thus hypothesize that differences in softness/flexibility of these polymeric nanoparticles could be responsible for their altered penetration behavior. The unsubstituted PGA polymer has a T_g much below room temperature (T_g −30 °C), thus at body temperature, it exists in a liquid-like state, i.e., it should form soft and flexible nanosystems.[47] However, an increase of substitution of PGA with C18 groups was shown to increase the T_g values due to a higher fatty acid chain interaction and high steric hindrance among polymer chains. This led to a higher rigidity of NPs[47] (Supporting Information Table S5 shows measured thermal properties and contact angles of PGA polymers). As already noted, model poly(styrene) NPs of comparable size have a penetration restricted to only 20% of the cell at the periphery of the spheroids (Supporting Information Figure S5). Poly(styrene) is a hard plastic which has a glass transition temperature (T_g) of ~90 °C, so at body temperature this material is in its glassy state, forming hard and rigid NPs. Thus, the slower penetration abilities of PGA-C18 NPs and poly(styrene) NPs could be a result of lower flexibility in comparison to unsubstituted PGA NPs (see Supporting Information Figure S5 for a direct comparison of poly(styrene) and PGA nanoparticle penetration). We hypothesize that the more flexible PGA systems are capable of deforming to squeeze through restricted spaces between the ECM fibers, providing more efficient penetration than the rigid NPs which end up being trapped in the ECM pores, restricting their diffusion. This hypothesis is in agreement with published observations on diffusion through a 2% agarose gel where semiflexible macromolecules were able to penetrate more efficiently through the gel than rigid spherical systems of the same hydrodynamic radius.[3,49,50]

The use of PEGylated-PGA nanoparticles was also investigated. PEG is a hydrophilic and neutral molecule which is often attached to the surface of liposomes and NPs. The steric effects and flexibility of the surface PEG layer reduce interactions of these systems with blood proteins, opsonins, and macrophages allowing for a longer circulation time.[51] By conjugating the PEG to unsubstituted PGA and PGA-C18, it was found that the resulting nanoparticles were capable of efficient penetration into the core of spheroids within a short time frame (2−6 h) and continued to accumulate up to 24 h. In particular, the addition of PEG to PGA-C18 significantly improved the penetration and accumulation of the system in spheroids. The presence of PEG on the surface of nanosystems is thought to reduce electrostatic interactions with ECM components thereby improving their diffusion.[52−54] There is very little difference between the surface charge of the PEGylated and non-PEGylated PGA-C18 NPs, but the presence of PEG may have had an effect on a variety of possible interactions between the NP surface and ECM, including those mediated by the presence of a protein corona. This is in agreement with previous studies which investigated the effect of the addition of PEG to charged nanoparticles in different ECM matrices and in mucus and found an improved penetration as a result.[52,55] Surface PEGylation of NPs > 100 nm was also shown to facilitate diffusion in the brain extracellular space.[54,56] In the case of PGA-C18, the penetration may have been further assisted by the effect of PEGylation of the polymer on the reduction of T_g and increased flexibility of the nanoparticle compared to non-PEGylated PGA-C18.

Different density and MW of PEG may also be a factor in achieving the maximal penetration into the tumor; however, this was not investigated in the present work.

DOI: 10.1021/acs.bioconjchem.9b00136
Bioconjugate Chem. 2019, 30, 1371−1384

While the present study gives us a good idea of the relative performance of different types of NPs, this is still a first step toward understanding how to design more successful delivery systems for tumors. Different tumors will have different combinations of host cells and tumor cells with different properties which are likely to affect both ECM and rates of endocytosis. Developing different models with different tumor cell types and in combination with host cells, e.g., fibroblasts and immune cells will further enhance the picture of how NPs penetrate tumors. It is noted, however, that cell cultures are relatively homogeneous cell populations, whereas in tumors the tumor cell heterogeneity may well play a further part in penetration, so further models with multiple cell types will be useful in extending our understanding of nanoparticle penetration into various types of tumors.

CONCLUSION

We have taken well-characterized HCT116 spheroids as a model system to compare the penetration of different NPs into tumors and investigated the effect of different composition and physicochemical features. We have employed Hoechst dye together with FACS to facilitate a quantitative assessment of penetration and distribution of nanoparticles in the spheroids. The method is highly sensitive and robust when compared to other methods used for the detection of nanoparticles within the core of spheroids such as microscopy or sequential trypsinisation.[27,57,58] It allows for fast detection of as few as 5−10 NPs per cell and provides a promising *in vitro* screening method for assessing nanoparticles in the early stages of their development.[24]

Our results highlight the need to control physicochemical features of nanoparticles such as size and surface charge when designing nanomedicines in order to achieve the best delivery of therapeutic agents into tumors.

METHODS

Materials. HCT 116 cells were obtained from the CRN NCI-60 cell bank initiative, Cancer Biology, Division of Cancer and Stem Cells, School of Medicine, University of Nottingham. K_i-67, BrdU, horseradish peroxidase rabbit-antimouse secondary antibody, and diaminobenzidin (DAB) were obtained from Pathology Products, Dako UK Ltd. (Ely, UK). Pimonidazole (Hypoxyprobe-1) was purchased from Hypoxyprobe, Inc. (Burlington, USA). Dulbecco's Phosphate Buffered Saline (PBS), L-glutamine solution (2 mM), RPMI-1640, Accutase Solution, Agarose, DPX mounting medium, and fast red solution were obtained from Sigma-Aldrich (Dorset, UK). Foetal Bovine Serum (FBS) solution was supplied by Invitrogen (Paisley, UK). Trypsin-EDTA was obtained from Gibco, Life Technologies Ltd. (Paisley, UK). Ultralow attachment 96-well round-bottom plates were obtained from Corning (UK). Paraformaldehyde solution (4%) and Alcian Blue were purchased from Alfa Aesar, a Johnson Matthey Company (Heysham, UK). Tissue-embedding cassettes were sourced from Simport (Beloeil, Canada). SuperFrost glass and poly-L-lysine coated slides were obtained from Menzel (Braunschweig, Germany). Vinyl specimen mold, CryomoldH, and Tissue-TekH O.C.T. compound were obtained from Tissue-Tek and Sakura Finetek (CA). Haematoxylin and Eosin were from Raymond Lamb (Eastbourne, UK). The Annexin V-FITC Apoptosis Detection Kit was purchased from eBioscience (Hatfield, UK). Hoechst 33342 (NucBlue Live ReadyProbes Reagent) was sourced from Life Technologies Ltd. (Paisley, UK). Doxorubicin (Adriamycin, Pfizer, UK) was provided by Cancer Biology Unit, Division of Cancer and Stem Cells University of Nottingham. PEGylated Liposomal doxorubicin hydrochloride (CAELYX) was purchased from Janssen (High Wycombe, UK). Rhodamine B isothiocyanate (RBITC) was purchased from Sigma-Aldrich (Poole, UK). Fluorescently labeled uniform plain poly(styrene) nanoparticles of sizes 30, 50, 100, 300, and 50 nm aminated and 50 nm carboxylated poly(styrene) nanoparticles were purchased from Magsphere Inc. (US) and used without further modification. Sephadex G-25 in PD-10 desalting columns were from GE Healthcare's Life Sciences solutions (Little Chalfont, UK).

Preparation of PGA NPS. Polymer synthesis: Poly(glycerol adipate) (PGA) was synthesized enzymatically from divinyl adipate and glycerol in DMF in the presence of Novozyme 435 at 50 °C, as described by Taresco et al.[36] PGA C18 was prepared by substitution of hydroxyl groups of PGA by reflux with acyl chloride in THF in the presence of pyridine. Full details for this synthesis can be found in Taresco et al.[39]

PEGylation of Polymers. In order to couple PEG chains (Mw = 2000 Da) to either PGA or PGAC18, a simple and consistent Steglich esterification was adopted by applying the same reaction conditions. Thus, the example (PGA−PEG) below can be applied to both the PGA−PEGylated modifications. Typically, PGA (1 g/0.1 mmol) and DMAP (0.015 mmol) were added to anhydrous THF (20 mL) at room temperature in a round-bottom flask under magnetic stirring until complete dissolution. In particular, since it is exclusively the end group of the PGA chain that takes part in this reaction, the whole molecular weight of the polymer was taken into consideration for any stoichiometry. A second solution was prepared by dissolving 0.15 mmol of dicyclohexyl carbodiimide and 0.15 mmol of PEG in THF (20 mL). The dicyclohexyl carbodiimide-PEG solution was poured into the polymer. The reaction was allowed to stir overnight. The resulting dicyclohexylurea was removed by centrifugation, and the supernatant solvent was removed under reduced pressure. The modified polymer was redissolved in THF and precipitated twice in cold MeOH. The residual material was dried under reduced pressure to a stable weight.

Nanoparticles from PGA and PGA derivatives were prepared by a nanoprecipitation method using acetone as a solvent as previously described by Meng et al.[43] Briefly, the polymer (5 mg) was dissolved in acetone (2 mL) containing RBITC (2 mg/mL), and the solution was added dropwise into HEPES buffer (5 mL). The mixture was left stirring overnight at room temperature to allow for acetone to evaporate. The unincorporated fluorescent dye from fluorescently labeled NPs was removed by Sephadex PD-10 Desalting Column using gravity flow according to the manufacturer protocol.

Characterization of Nanoparticles. Zetasizer Nano-ZS (Malvern Instruments, Worcestershire, UK) was used to measure size distribution, Z potential, and polydispersity index of nanoparticles. Experiments were conducted at 25 °C after diluting the nanoparticles to 200 μg/mL in 10 mM HEPES, RPMI-1640 medium, and RPMI-1640 medium supplemented with 10% FBS.

Spheroid Culture. Ultra low attachment 96-well round-bottom plates were employed for the culturing of spheroids. Cells grown as a monolayer were detached using trypsin and then centrifuged, and the cell number was counted using a

DOI: 10.1021/acs.bioconjchem.9b00136
Bioconjugate Chem. 2019, 30, 1371−1384

hemocytometer. Spheroids were seeded by diluting the single-cell suspensions in a RPMI-1640 medium with 10% FBS and 10^4 cells per mL were added at a constant volume (200 μL) per well in 96-well ultra low attachment plates. Six wells containing the same concentration of cells were created for the experiments. The plates were centrifuged at 100g for 4 min. The medium (150 μL) was removed on days 3 and 5 and replaced with fresh medium.

Growth of HCT116 Spheroids. Spheroids were imaged daily for 7 days using a Nikon Eclipse Ti microscope with a 4× objective (Nikon limited, Surrey, UK). The pictures were analyzed using image J and a macro written by Ivanov et al.[35] The diameter and volume of spheroids were determined by measuring their cross-sectional area.

Immunochemical Analysis of HCT116 Spheroids. Prior to processing, spheroids were fixed using paraformaldehyde solution (4%) in PBS for 1 h. Prior to wax embedding, fixed spheroids were transferred to the top of a solidified agarose gel (1.5%, 200 μL) in 1.5 mL microcentrifuge tubes. The spheroids were allowed to sediment on top of the agarose gel, and supernatant was removed by gentle aspiration. Warm liquid agarose (1% w/v in sterile water, ∼100 μL) was gently added on top of the spheroids and left to set. Once solidified, the tip of the microcentrifuge tube was excised using a blade, and the piece of the agarose containing the spheroids was transferred into tissue embedding cassettes and were processed using a routine paraffin embedding technique (Leica EG1160, Milton Keynes, UK). Sections of 4 μm were cut using a microtome (Leica RM2135), placed on Super Frost glass slides. The prepared slides were stained with Haematoxylin and Eosin (H&E) and Alcian Blue (pH 2.5)/fast red as per standard protocol. K_i-67 was used for staining of proliferating cells; mouse-antihuman K_i-67 clone MIB-1 (46 mg/L; 1:200 in PBS) was used followed by incubation with horseradish peroxidase-rabbit-antimouse secondary antibody (1.3 g/L) at 1:300 dilution followed by DAB staining. Citric acid buffer at pH 6 and 98 °C for 30 min was used for antigen retrieval. Hypoxia detection was performed by using pimonidazole hypochloride. Spheroids were incubated for 2 h with PIMO at a 100 μM final concentration in the media. The spheroids were then fixed and processed for frozen sections. Pimonidazole adducts were detected by incubating sections with fluorescein isothiocyanate-conjugated MAb1 (monoclonal antibody as provided by the supplier, 1:300) for 2 h at 37 °C. The sections were counterstained with hematoxylin. The slides were coverslipped with DPX and air-dried overnight, and spheroid sections were assessed by microscopy (Leica DMLB).

Penetration and Uptake of Nanoparticles into Spheroid Model. Spheroids were grown on ultra low attachment plates for 3 days to allow for compaction prior to use for the penetration and uptake studies. On day 3 of the culture, the media were removed from the wells and replaced with media (150 μL) containing NPs (75 μg/mL) or DOX (1 μg/mL or 10 μg/mL or 75 μg/mL as Caelyx) and were left to incubate for 2−24 h. Four hours prior to the end of the incubation, Hoechst was added to the wells (final concentration in the well = 0.1 μM) and was left to incubate. At the end of the incubation, the spheroids were washed three times with PBS and fixed with 4% paraformaldehyde for 1 h then processed for frozen sections.

Evaluating the Penetration of Fluorescent Poly(styrene) Nanoparticles by Confocal Microscopy. After fixation, spheroids were incubated in 30% sucrose in PBS overnight at 4 °C. Spheroids were transferred onto a vinyl specimen mold. The remaining sucrose solution was aspirated, and the tissue-TekH O.C.T. compound was gently poured over the spheroids. The spheroids were then submerged in an isopentane bath cooled by dry ice and cut into 20-μm-thick sections using a cryostat microtome. The sections were mounted onto superfrost glass slides and were gently immersed in PBS to remove the remaining OCT compound. Subsequently, the frozen sections of spheroids incubated with NPs were examined by confocal microscopy (laser 538) and by image J software. The sections from the middle of a minimum of two independent spheroids per experiment were selected based on the degree of Hoechst staining, and the experiment was repeated twice. In image J, the images were pseudocolored with mask LUT "fire" that reflects differences in intensity of the nanoparticles within spheroids.

Evaluating the Penetration and Uptake of Fluorescent Poly(styrene) Nanoparticles by Flow Cytometry. After incubation of spheroids with NPs for 2, 4, 6, and 24 h and Hoechst 33342 (0.1 μM) for 4 h, the spheroids were transferred into 15 mL Falcon conical tubes and washed twice with PBS (1 mL). Accutase (1 mL, 400−600 units/mL) was then added, and the tubes incubated at 37 °C for 3 min with agitation. The dissociation of spheroids was aided by mechanical pipetting. The spheroids were then centrifuged, fixed, and washed in PBS and subsequently analyzed by flow cytometry (MoFlo Astrios Cell sorter, Beckman Coulter). A blue laser at 355−488 nm and a yellow/green laser at 488−664 nm were used as an excitation source for the detection of Hoechst and nanoparticle fluorescence, respectively. Samples were analyzed with the Kaluza Analysis 1.3 Software. Cells-only control was used to set the threshold for cells without NPs. Cells were divided into three cell populations representing the rim, middle, and core of spheroid based on the intensity of staining with Hoechst, 20%, 40%, and 40% of total cells, respectively. (As the divisions are created manually, there is a small variation in the sizes of the different divisions.) The difference in mean fluorescence intensity (MFI) between the data was normalized by designating one NP in a set to equal 1 and applying that adjustment factor to remaining NPs by use of ratiometric results.

Statistical Analysis. Unless otherwise stated, all data are shown as mean ± standard deviation (SD; n = number of spheroids per experiment). One way analysis of variance (ANOVA) was applied for comparison of three or more group means. A P value of < 0.05 was considered statistically significant. ****, ***, **, and * display $p < 0.0001$, $p < 0.001$, $p < 0.01$, and $p < 0.05$, respectively. GraphPad Prism 6 software was used for data analysis.

■ ASSOCIATED CONTENT

Supporting Information

The Supporting Information is available free of charge on the ACS Publications website at DOI: 10.1021/acs.bioconjchem.9b00136.

Figures S1−S5, Tables S1−S5, calculations on DOX availability in spheroids (PDF)

■ AUTHOR INFORMATION

Corresponding Author

*Tel.: +44 1159515045. E-mail: martin.garnett@nottingham.ac.uk.

DOI: 10.1021/acs.bioconjchem.9b00136
Bioconjugate Chem. 2019, 30, 1371−1384

ORCID

Vincenzo Taresco: 0000-0003-4476-8233
Snow Stolnik: 0000-0002-2345-5062
Martin C. Garnett: 0000-0002-4365-4499

Author Contributions

The manuscript was written through contributions of all authors. All authors have given approval to the final version of the manuscript.

Funding

This research was supported by an Engineering and Physical Sciences Research Council Centre for Doctoral Training in Targeted Therapeutics and formulation science (EP/I01375X/1) in a project supported by AstraZeneca.

Notes

The authors declare no competing financial interest.

■ ACKNOWLEDGMENTS

Grateful acknowledgements for the technical assistance from the teams at Cancer Biology (D. Ivanov, P. Clarke, P. Collier); Advanced Microscopy Unit (I. Ward, D. Mclean, S. Rajani); and Flow Cytometry Facility team (D. Onion, N. Croxall) at QMC, University of Nottingham. Also thanks to S. Swainson for assistance with the PGA polymers and nanoparticles.

■ ABBREVIATIONS

C18, oleate; DAB, diaminobenzidine; Dox, doxorubicin; ECM, extracellular matrix; FACS, fluorescence activated cell sorter; FBS, fetal bovine serum; HEPES, hydroxyethyl piperazine ethyl sulfonate; MFI, mean fluorescence intensity; NP, nanoparticle; PBS, Dulbecco's phosphate buffered saline; PEG, poly(ethylene glycol); PGA, poly(glycerol adipate)

■ REFERENCES

(1) Barua, S., and Mitragotri, S. (2014) Challenges Associated with Penetration of Nanoparticles across Cell and Tissue Barriers: A Review of Current Status and Future Prospects. *Nano Today 9*, 223−243.

(2) Tang, L., Gabrielson, N. P., Uckun, F. M., Fan, T. M., and Cheng, J. (2013) Size-Dependent Tumor Penetration and in Vivo Efficacy of Monodisperse Drug-Silica Nanoconjugates. *Mol. Pharmaceutics 10*, 883−892.

(3) Jain, R. K., and Stylianopoulos, T. (2010) Delivering Nanomedicine to Solid Tumors. *Nat. Rev. Clin. Oncol. 7*, 653−664.

(4) Minchinton, A. I., and Tannock, I. F. (2006) Drug Penetration in Solid Tumours. *Nat. Rev. Cancer 6*, 583−592.

(5) Magzoub, M., Jin, S., and Verkman, A. S. (2008) Enhanced Macromolecule Diffusion Deep in Tumors after Enzymatic Digestion of Extracellular Matrix Collagen and Its Associated Proteoglycan Decorin. *FASEB J. 22*, 276−284.

(6) Dreher, M. R., Liu, W., Michelich, C. R., Dewhirst, M. W., Yuan, F., and Chilkoti, A. (2006) Tumor Vascular Permeability, Accumulation, and Penetration of Macromolecular Drug Carriers. *J. Natl. Cancer Inst. 98*, 335−344.

(7) Steichen, S. D., Caldorera-Moore, M., and Peppas, N. A. (2013) A Review of Current Nanoparticle and Targeting Moieties for the Delivery of Cancer Therapeutics. *Eur. J. Pharm. Sci. 48*, 416−427.

(8) Jain, R. K. (1987) Transport of Molecules in the Tumor Interstitium: A Review. *Cancer Res. 47*, 3039−3051.

(9) Comper, W. D., and Laurent, T. C. (1978) Physiological Function of Connective Tissue Polysaccharides. *Physiol. Rev. 58*, 255−315.

(10) Laurent, T. C., and Ogston, A. G. (1963) The Interaction between Polysaccharides and Other Macromolecules 4. The Osmotic Pressure of Mixtures of Serum Albumin and Hyaluronic Acid. *Biochem. J. 89*, 249−253.

(11) Ogston, A. G., and Sherman, T. F. (1961) Effects of Hyaluronic Acid upon Diffusion of Solutes and Flow of Solvent. *J. Physiol. 156*, 67−74.

(12) Netti, P. A., Berk, D. A., Swartz, M. A., Grodzinsky, A. J., and Jain, R. K. (2000) Role of Extracellular Matrix Assembly in Interstitial Transport in Solid Tumors. *Cancer Res. 60*, 2497−2503.

(13) Goodman, T. T., Olive, P. L., and Pun, S. H. (2007) Increased Nanoparticle Penetration in Collagenase-Treated Multicellular Spheroids. *Int. J. Nanomedicine 2*, 265−274.

(14) Pluen, A., Boucher, Y., Ramanujan, S., McKee, T. D., Gohongi, T., di Tomaso, E., Brown, E. B., Izumi, Y., Campbell, R. B., Berk, D. A., et al. (2001) Role of Tumor-Host Interactions in Interstitial Diffusion of Macromolecules: Cranial vs. Subcutaneous Tumors. *Proc. Natl. Acad. Sci. U. S. A. 98*, 4628−4633.

(15) Stylianopoulos, T., Poh, M.-Z., Insin, N., Bawendi, M. G., Fukumura, D., Munn, L. L., and Jain, R. K. (2010) Diffusion of Particles in the Extracellular Matrix: The Effect of Repulsive Electrostatic Interactions. *Biophys. J. 99*, 1342−1349.

(16) Lieleg, O., Baumgärtel, R. M., and Bausch, A. R. (2009) Selective Filtering of Particles by the Extracellular Matrix: An Electrostatic Bandpass. *Biophys. J. 97*, 1569−1577.

(17) Wenzel, C., Riefke, B., Gründemann, S., Krebs, A., Christian, S., Prinz, F., Osterland, M., Golfier, S., Räse, S., Ansari, N., et al. (2014) 3D High-Content Screening for the Identification of Compounds That Target Cells in Dormant Tumor Spheroid Regions. *Exp. Cell Res. 323*, 131−143.

(18) Unger, C., Kramer, N., Walzl, A., Scherzer, M., Hengstschläger, M., and Dolznig, H. (2014) Modeling Human Carcinomas : Physiologically Relevant 3D Models to Improve Anti-Cancer Drug Development. *Adv. Drug Delivery Rev. 79−80*, 50−67.

(19) Leong, D. T., and Ng, K. W. (2014) Probing the Relevance of 3D Cancer Models in Nanomedicine Research. *Adv. Drug Delivery Rev. 79−80*, 95−106.

(20) Thoma, C. R., Zimmermann, M., Agarkova, I., Kelm, J. M., and Krek, W. (2014) 3D Cell Culture Systems Modeling Tumor Growth Determinants in Cancer Target Discovery. *Adv. Drug Delivery Rev. 69−70*, 29−41.

(21) Hirschhaeuser, F., Menne, H., Dittfeld, C., West, J., Mueller-Klieser, W., and Kunz-Schughart, L. A. (2010) Multicellular Tumor Spheroids: An Underestimated Tool Is Catching up Again. *J. Biotechnol. 148*, 3−15.

(22) Vinci, M., Gowan, S., Boxall, F., Patterson, L., Zimmermann, M., Court, W., Lomas, C., Mendiola, M., Hardisson, D., and Eccles, S. A. (2012) Advances in Establishment and Analysis of Three-Dimensional Tumor Spheroid-Based Functional Assays for Target Validation and Drug Evaluation. *BMC Biol. 10*, 29.

(23) Ivascu, A., and Kubbies, M. (2006) Rapid Generation of Single-Tumor Spheroids for High-Throughput Cell Function and Toxicity Analysis. *J. Biomol. Screening 11*, 922−932.

(24) Mikhail, A. S., Eetezadi, S., and Allen, C. (2013) Multicellular Tumor Spheroids for Evaluation of Cytotoxicity and Tumor Growth Inhibitory Effects of Nanomedicines in Vitro: A Comparison of Docetaxel-Loaded Block Copolymer Micelles and Taxotere®. *PLoS One 8*, e62630.

(25) Ivanov, D. P., Parker, T. L., Walker, D. A., Alexander, C., Ashford, M. B., Gellert, P. R., and Garnett, M. C. (2014) Multiplexing Spheroid Volume, Resazurin and Acid Phosphatase Viability Assays for High-Throughput Screening of Tumour Spheroids and Stem Cell Neurospheres. *PLoS One 9*, e103817.

(26) Lee, H., Fonge, H., Hoang, B., Reilly, R. M., and Allen, C. (2010) The Effects of Particle Size and Molecular Targeting on the Intratumoral and Subcellular Distribution of Polymeric Nanoparticles. *Mol. Pharmaceutics 7*, 1195−1208.

(27) Durand, R. E. (1982) Use of Hoechst 33342 for Cell Selection from Muticell Systems. *J. Histochem. Cytochem. 30*, 117−122.

DOI: 10.1021/acs.bioconjchem.9b00136
Bioconjugate Chem. 2019, 30, 1371−1384

(28) Gabizon, A., Shmeeda, H., and Barenholz, Y. (2003) Pharmacokinetics of Pegylated Liposomal Doxorubicin: Review of Animal and Human Studies. *Clin. Pharmacokinet. 42*, 419−436.
(29) Ren, S., Li, C., Dai, Y., Li, N., Wang, X., Tian, F., Zhou, S., Qiu, Z., Lu, Y., Zhao, D., et al. (2014) Comparison of Pharmacokinetics, Tissue Distribution and Pharmacodynamics of Liposomal and Free Doxorubicin in Tumour-Bearing Mice Following Intratumoral Injection. *J. Pharm. Pharmacol. 66*, 1231−1239.
(30) Meng, W., Garnett, M. C., Walker, D. A., and Parker, T. L. (2016) Penetration and Intracellular Uptake of Poly(Glycerol-Adipate) Nanoparticles into Three-Dimensional Brain Tumour Cell Culture Models. *Exp. Biol. Med. 241*, 466−477.
(31) Eikenes, L., Tari, M., Tufto, I., Bruland, O. S., and de Lange Davies, C. (2005) Hyaluronidase Induces a Transcapillary Pressure Gradient and Improves the Distribution and Uptake of Liposomal Doxorubicin (Caelyx) in Human Osteosarcoma Xenografts. *Br. J. Cancer 93*, 81−88.
(32) López-Dávila, V., Magdeldin, T., Welch, H., Dwek, M. V., Uchegbu, I., and Loizidou, M. (2016) Efficacy of DOPE/DC-Cholesterol Liposomes and GCPQ Micelles as AZD6244 Nanocarriers in a 3D Colorectal Cancer in Vitro Model. *Nanomedicine 11*, 331−344.
(33) Cabral, H., Matsumoto, Y., Mizuno, K., Chen, Q., Murakami, M., Kimura, M., Terada, Y., Kano, M. R., Miyazono, K., Uesaka, M., et al. (2011) Accumulation of Sub-100 Nm Polymeric Micelles in Poorly Permeable Tumours Depends on Size. *Nat. Nanotechnol. 6*, 815−823.
(34) Huang, K., Ma, H., Liu, J., Huo, S., Kumar, A., Wei, T., Zhang, X., Jin, S., Gan, Y., Wang, P. C., et al. (2012) Size-Dependent Localization and Penetration of Ultrasmall Gold Nanoparticles in Cancer Cells, Multicellular Spheroids, and Tumors in Vivo. *ACS Nano 6*, 4483−4493.
(35) Bugno, J., Hsu, H.-J., Pearson, R. M., Noh, H., and Hong, S. (2016) Size and Surface Charge of Engineered Poly(Amidoamine) Dendrimers Modulate Tumor Accumulation and Penetration: A Model Study Using Multicellular Tumor Spheroids. *Mol. Pharmaceutics 13*, 2155−2163.
(36) Bao, A., Phillips, W. T., Goins, B., Zheng, X., Sabour, S., Natarajan, M., Ross Woolley, F., Zavaleta, C., and Otto, R. A. (2006) Potential Use of Drug Carried-Liposomes for Cancer Therapy via Direct Intratumoral Injection. *Int. J. Pharm. 316*, 162−169.
(37) Ashton, S., Song, Y. H., Nolan, J., Cadogan, E., Murray, J., Odedra, R., Foster, J., Hall, P. A., Low, S., Taylor, P., et al. (2016) Aurora Kinase Inhibitor Nanoparticles Target Tumors with Favorable Therapeutic Index in Vivo. *Sci. Transl. Med. 8*, 325ra17.
(38) Tannock, I. F., Lee, C. M., Tunggal, J. K., Cowan, D. S. M., and Egorin, M. J. (2002) Limited Penetration of Anticancer Drugs through Tumor Tissue: A Potential Cause of Resistance of Solid Tumors to Chemotherapy. *Clin. Cancer Res. 8*, 878−884.
(39) Lundqvist, M., Stigler, J., Elia, G., Lynch, I., Cedervall, T., and Dawson, K. A. (2008) Nanoparticle Size and Surface Properties Determine the Protein Corona with Possible Implications for Biological Impacts. *Proc. Natl. Acad. Sci. U. S. A. 105*, 14265−14270.
(40) Juweid, M., Neumann, R., Paik, C., Perez-Bacete, M. J., Sato, J., Van Osdol, W., and Weinstein, J. N. (1992) Micropharmacology of Monoclonal Antibodies in Solid Tumors: Direct Experimental Evidence for a Binding Site Barrier. *Cancer Res. 52*, 5144−5153.
(41) Goodman, T. T., Chen, J., Matveev, K., and Pun, S. H. (2008) Spatio-Temporal Modeling of Nanoparticle Delivery to Multicellular Tumor Spheroids. *Biotechnol. Bioeng. 101*, 388−399.
(42) Weiss, V. M., Naolou, T., Hause, G., Kuntsche, J., Kressler, J., and Mäder, K. (2012) Poly(Glycerol Adipate)-Fatty Acid Esters as Versatile Nanocarriers: From Nanocubes over Ellipsoids to Nanospheres. *J. Controlled Release 158*, 156−164.
(43) Meng, W., Parker, T. L., Kallinteri, P., Walker, D. A., Higgins, S., Hutcheon, G. A., and Garnett, M. C. (2006) Uptake and Metabolism of Novel Biodegradable Poly(Glycerol-Adipate) Nanoparticles in DAOY Monolayer. *J. Controlled Release 116*, 314−321.
(44) Meng, W., Kallinteri, P., Walker, D., Parker, T. L., and Garnett, M. C. (2007) Evaluation of Poly (Glycerol-Adipate) Nanoparticle Uptake in an in Vitro 3-D Brain Tumor Co-Culture Model. *Exp. Biol. Med. 232*, 1100−1108.
(45) Kallinteri, P., Higgins, S., Hutcheon, G. A., St. Pourçain, C. B., and Garnett, M. C. (2005) Novel Functionalized Biodegradable Polymers for Nanoparticle Drug Delivery Systems. *Biomacromolecules 6*, 1885−1894.
(46) Puri, S., Kallinteri, P., Higgins, S., Hutcheon, G. A., and Garnett, M. C. (2008) Drug Incorporation and Release of Water Soluble Drugs from Novel Functionalised Poly(Glycerol Adipate) Nanoparticles. *J. Controlled Release 125*, 59−67.
(47) Taresco, V., Suksiriworapong, J., Creasey, R., Burley, J. C., Mantovani, G., Alexander, C., Treacher, K., Booth, J., and Garnett, M. C. (2016) Properties of Acyl Modified Poly(Glycerol-Adipate) Comb-Like Polymers and Their Self-Assembly into Nanoparticles. *J. Polym. Sci., Part A: Polym. Chem. 54*, 3267−3278.
(48) Mackenzie, R., Booth, J., Alexander, C., Garnett, M. C., and Laughton, C. A. (2015) Multiscale Modeling of Drug−Polymer Nanoparticle Assembly Identifies Parameters Influencing Drug Encapsulation Efficiency. *J. Chem. Theory Comput. 11*, 2705−2713.
(49) Pluen, A., Netti, P. A., Jain, R. K., and Berk, D. A. (1999) Diffusion of Macromolecules in Agarose Gels: Comparison of Linear and Globular Configurations. *Biophys. J. 77*, 542−552.
(50) Nugentand, L. J., and Jain, R. (1984) Extravascular Diffusion in Normal and Neoplastic Tissues. *Cancer Res. 44*, 238−244.
(51) Stolnik, S., Illum, L., and Davis, S. S. (1995) Long Circulating Microparticulate Drug Carriers. *Adv. Drug Delivery Rev. 16*, 195−214.
(52) Tomasetti, L., Liebl, R., Wastl, D. S., and Breunig, M. (2016) Influence of PEGylation on Nanoparticle Mobility in Different Models of the Extracellular Matrix. *Eur. J. Pharm. Biopharm. 108*, 145−155.
(53) Pirollo, K. F., and Chang, E. H. (2008) Does a Targeting Ligand Influence Nanoparticle Tumor Localization or Uptake? *Trends Biotechnol. 26*, 552−558.
(54) Waite, C. L., and Roth, C. M. (2012) Nanoscale Drug Delivery Systems for Enhanced Drug Penetration into Solid Tumors: Current Progress and Opportunities. *Crit. Rev. Biomed. Eng. 40*, 21−41.
(55) Mun, E. A., Hannell, C., Rogers, S. E., Hole, P., Williams, A. C., and Khutoryanskiy, V. V. (2014) On the Role of Specific Interactions in the Diffusion of Nanoparticles in Aqueous Polymer Solutions. *Langmuir 30*, 308−317.
(56) Nance, E. A., Woodworth, G. F., Sailor, K. A., Shih, T.-Y., Xu, Q., Swaminathan, G., Xiang, D., Eberhart, C., and Hanes, J. (2012) A Dense Poly(Ethylene Glycol) Coating Improves Penetration of Large Polymeric Nanoparticles Within Brain Tissue. *Sci. Transl. Med. 4*, 149ra119.
(57) Trotter, M. J., Olive, P. L., and Chaplin, D. J. (1990) Effect of Vascular Marker Hoechst 33342 on Tumour Perfusion and Cardiovascular Function in the Mouse. *Br. J. Cancer 62*, 903−908.
(58) Sims, L. B., Curtis, L. T., Frieboes, H. B., and Steinbach-Rankins, J. M. (2016) Enhanced Uptake and Transport of PLGA-Modified Nanoparticles in Cervical Cancer. *J. Nanobiotechnol. 14*, 33.

DOI: 10.1021/acs.bioconjchem.9b00136
Bioconjugate Chem. 2019, 30, 1371−1384